Particle-in-cell simulation method for degenerate plasmas

D. Wu,[1,*] W. Yu,[2] S. Fritzsche,[3,4] and X. T. He[1,5]

[1] *Institute for Fusion Theory and Simulation, Department of Physics, Zhejiang University, 310058 Hangzhou, China*
[2] *Shanghai Institute of Optics and Fine Mechanics, 201800 Shanghai, China*
[3] *Helmholtz Institut Jena, D-07743 Jena, Germany*
[4] *Theoretisch-Physikalisches Institut, Friedrich-Schiller-University Jena, D-07743 Jena, Germany*
[5] *Key Laboratory of HEDP of the Ministry of Education, CAPT, and State Key Laboratory of Nuclear Physics and Technology, Peking University, 100871 Beijing, China*

(Dated: December 4, 2019)

Nowadays radiation hydrodynamic equations coupled with external equation of state provided by quantum mechanical calculations is an intensively investigated approach for simulations of degenerate plasmas. Although such an approach is proven to be efficient and shows many good features, specially for large scale simulations, it encounters intrinsic challenges when involving kinetic effects. As a complement, we here have invented a fully kinetic numerical approach for simulations of plasmas with an arbitrary degeneracy level. This approach is based on first principle Boltzmann equation coupled with Maxwell's equations and a complicated collision operator, and is eventually achieved via an existing particle-in-cell simulation code named LAPINS. In this approach, degenerate particles are initialized according to a Fermi-Dirac distribution function, and non-degenerate particles are initialized following typical Maxwell distribution function. The equation of motion of both degenerate and non-degenerate particles are governed by long range collective electromagnetic fields and close particle-particle scatterings with degeneracy corrections. Especially, the evolutions of degenerate particles are also constrained by the Pauli exclusion principle. The code is applied to several benchmark simulations, including electronic conductivity for aluminium with temperature from $0-50$ eV, equilibration of cold fuel shell and alpha particles in inertial confinement fusion, and rapid heating of solid aluminium by intense laser beams.

PACS numbers: 52.38.Kd, 41.75.Jv, 52.35.Mw, 52.59.-f

I. INTRODUCTION

Modelling degenerate plasmas is among the key investigation efforts for high energy density physics studies, which is of significant importances to inertial confinement fusion (ICF), astrophysical, and laboratory astrophysical studies, for example, compression of the cold fuel and capsule shell [1, 2], white dwarf starts [3], and high power laser solid interaction experiments [4–7].

For degenerate plasmas, density functional theory-molecular dynamics (DFT-MD) method [8–13] is intensively investigated. This method is though to be accurate however is limited in the problems it can be applied to due to its significant computational expense. Radiation hydrodynamic simulation [14, 15] coupled with external equation of state data provided by DFT-MD calculations is a nowadays widely applied approach. Although such an approach is proven to be efficient and shows many good features, specially for large scale simulations, it encounters intrinsic challenges when involving kinetic effects, for example, degenerate thermal equilibration and the stopping of high energy alpha particles by degenerate electrons in ICF.

The particle-in-cell (PIC) method [16] has established itself as a state of the art method for solving problems in kinetic plasma physics. It is a compromise between fundamental quantum mechanical simulations, i.e. DFT-MD, and macro-field only methods, i.e., radiation hydrodynamic simulations. The main advantages of the PIC method are that their memory consumption increases linearly with the simulated volume and that the runtime is only of order N. They are also very suitable for the use of large multi-processor systems. Although the present PIC method is very successful in a great variety of research branches, when referring to degenerate plasmas, tremendous challenges still remain. For degenerate plasmas, usually, the electron density is more than solid density. However the main disadvantages of PIC method are high noise levels and high computational requirements for plasmas at solid densities. Within simulations, plasma frequency needs to be resolved, and the grid size must be comparable to the Debye length in order to minimize artificial grid heating and suppress numerical instabilities. In addition to tremendous simulation burdens, degenerate particles can no longer be regarded as classically distinguishable, and they obey Fermi-Dirac statistics. However, whether the PIC method based on classically distinguishable macro-particles is able to manipulate Fermi-Dirac rules is still open.

On the positive side, higher order interpolation algorithms have long been utilized in explicit PIC method, which is, to some extent, successful in suppressing artificial grid heating and suppress numerical instabilities. However for degenerate plasmas, usually the electron density can be as high as 10^{24} cm^{-3}, challenges still remain for high order explicit PIC methods. Recently, we

* Email: dwu.phys@zju.edu.cn

proposed a high order interpolation implicit PIC method for plasma simulations at solid densities [17], and implemented in the LAPINS code. This is achieved by combining a high-order scheme of special difference with an implicit scheme of temporal stepping. This new scheme can completely remove the numerical self-heating and significantly reduce the simulation burden when simulating solid density plasmas. In the meanwhile, another numerical method that combines the PIC method with a reduced model of high density plasma based on Ohm's law was also proposed [18], implemented and benchmarked in the LAPINS code. Here, the electric field is solved via $\mathbf{E} = \eta \mathbf{J}_{\rm bg} - \mathbf{u}_{\rm bg} \times \mathbf{B}$, with η, $\mathbf{J}_{\rm bg}$, and $\mathbf{u}_{\rm bg}$ the conductivity, current density and average velocity of background plasmas, respectively. This method is proven to be efficient and a good choice for transport studies of energetic particles in solid density plasmas, provided the high frequency electromagnetic fields are not of significance.

For solid density plasmas, when the temperature is lower than the Fermi temperature, degeneracy effect appears. Actually this effect has long been noticed in PIC simulations for solid density plasmas. For example, to avoid a divergence of the Spitzer collision frequency in cold plasma, Sentoku [19] set a threshold of plasma temperature $T_{\rm tr}$ for a degenerate plasma. Collision frequency with energy less than $T_{\rm tr}$ is cut off with a constant value.

Here in this paper, we have invented a self-consistent kinetic approach for simulation of plasmas with an arbitrary degeneracy level. This approach is based on first principle Boltzmann equation coupled with Maxwell's equations and a complicated collision operator, and is eventually achieved via an existing particle-in-cell simulation code named LAPINS. With this approach, degenerate particles are initialized according to a Fermi-Dirac distribution function, and non-degenerate particles are initialized following typical Maxwell distribution function. The equation of motion of both degenerate and non-degenerate particles are governed by long range collective electromagnetic fields and close particle-particle scatterings with degeneracy corrections. Especially, evolutions of degenerate particles are also constrained by the Pauli exclusion principle. In the end, LAPINS code is applied to several benchmark simulations, which includes electronic conductivity for aluminium with varying temperatures, equilibration alpha particles with cold fuel shell in ICF, and rapid heating of solid aluminium by intense laser beams.

The paper is organized as follows. In Sec. II, the basic theoretical framework, i.e., Boltzmann equation coupled with Maxwell's equations and a complicated collision operator is outlined. Section III is the core part of this paper. Fermi-Dirac distribution initialization of degenerate particles along with the implementation of Pauli exclusion principle is presented. Moreover, the degeneracy corrected collision model and ionization model are also briefly discussed. In section IV, we present several simulation experiments to benchmark this new approach. Finally, summary and discussion are given in Sec. V.

II. BOLTZMANN EQUATIONS

In Boltzmann theory, a plasmas consisting of electrons and ions is represented by distribution functions f_k of seven variables, i.e., the position $\mathbf{r}$, velocity $\mathbf{u}$, and time t. The distribution function f_k gives the probability $f_k(\mathbf{r}, \mathbf{u}, t) d\mathbf{r} d\mathbf{u}$ of finding particles of k species in a given volume of six-dimensional phase space $d\mathbf{r}d\mathbf{u}$. The electrons and ions in plasma under consideration interact via long range electromagnetic fields and close binary collisions. Hence, an appropriate description of the plasma is based on the following Boltzmann equation,

$$\frac{\partial f_k}{\partial t} + \mathbf{u}_k \cdot \frac{\partial f_k}{\partial \mathbf{r}} - \frac{q_k}{m_k}(\mathbf{E} + \mathbf{u}_k \times \mathbf{B}) \cdot \frac{\partial f_k}{\partial \mathbf{u}_k} = \frac{\partial f_k}{\partial t}|_{\rm coll}, \quad (1)$$

where $\mathbf{E}$ and $\mathbf{B}$ are the electric and magnetic fields, and q_k is the value of particle charge, and m_k is the particle mass. The Maxwell's Equations read,

$$\nabla \times \mathbf{E} = -\partial_t \mathbf{B}, \quad (2)$$

$$\nabla \times \mathbf{B} = \partial_t \mathbf{E} + 2\pi \mathbf{J}, \quad (3)$$

$$\nabla \cdot \mathbf{E} = 2\pi\rho. \quad (4)$$

Boltzmann equation, Eq. (1), is coupled with Maxwell's equations via charge density ρ and current density $\mathbf{J}$, defined as

$$\rho(\mathbf{r}) = \sum_k q_k \int d^3 u_k f_k, \quad (5)$$

$$\mathbf{J}(\mathbf{r}) = \sum_k q_k \int d^3 u_k \mathbf{u}_k f_k. \quad (6)$$

In Eq. (1), $\partial f_k/\partial t|_{\rm coll}$ is the rate of change of the distribution function due to scatterings, which includes contributions from both the same species, e.g. electron-electron and ion-ion scatterings, and the different species, e.g. electron-ion and electron-neutral scatterings.

In principle, the distribution function f_k can be of any form, provided the normalization condition is satisfied. For ideal plasmas, under local equilibrium, f_k obeys Maxwell distribution $f_k \sim \exp(-E_k/T_k)$, with E_k of energy and T_k of temperatures. As an alternative solution of coupled Eqs. (1)-(6), plasma physicists have developed the PIC method based on the theory of charge assignment and force interpolation. This important theory has made it possible to obtain smooth distributions of charge density and current density in Maxwell's equation of electromagnetic fields. The PIC method, including the Monte Carlo (MC) treatment of collisions, is called the PIC/MC method. Takizuka and Abe [20] used to proposed a Monte Carlo approach for collisions, based on the binary collision approximation. In this approach, particles are randomly paired with each other in close proximity and scattered with Coulomb collisions, each one of which conserves energy and momentum. Apart from conservation, the greatest strength of this approach is the ability to work with any distribution function, especially

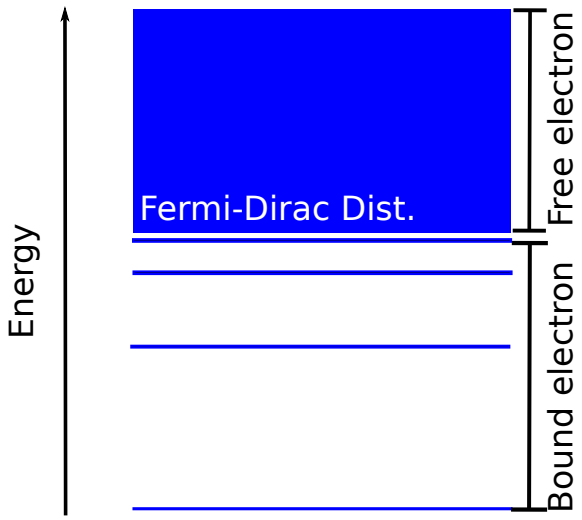

FIG. 1. (color online) Schematic representation for energy levels of degenerate plasma in the LAPINS PIC code. The electrons are classified, into bound and free ones, where the former are regarded as part of ions or atoms, and the latter are isolated as the surrounding plasmas. Free electrons and bound electrons can interchange with each other trough ionization and recombination processes. The energy distribution of free electrons is described by Fermi-Dirac statistics. Ions or atoms along with the bound electrons are treated as classical particles and obey Maxwell statistics.

those which depart appreciably from a Maxwell distribution. It has been extended several times for example by Sentoku [19], Wu [21] and Turrell [22] with arbitrary particle weight, inelastic scatterings and degeneracy corrections.

III. NUMERICAL IMPLEMENTATION

Boltzmann equation indicates that f_k in Eq. (1) can be of any form, provided normalization condition is satisfied. In order to simulate degenerate plasmas, here we have invented a fully kinetic numerical approach that can be configured and embedded into existing PIC simulation codes. In this approach, as schematically displayed in Fig. 1, we use a collection of macro-particles to describe a plasma or matter of finite ion density. Here, a macro-particle can be regarded as the ensemble of real particles, i.e., a group of particles with same mass, charge state, position, and momentum. The electrons are classified, moreover, into bound and free ones, where the former are regarded as part of ions or atoms, and the latter are isolated as the surrounding plasmas. Especially, free electrons and bound electrons can interchange with each other trough ionization and recombination processes. While ions or atoms along with the bound electrons are treated as classical particles and obey Maxwell statistics, free electrons in our method are dominated by Fermi-Dirac statistics.

A. Fermi-Dirac Statistics of Electrons

For degenerate plasmas, due to the anti-commutation relation for identical fermions, the distribution function for electrons obey Fermi-Dirac distribution,

$$f_e(E) = \frac{(2m_e)^{3/2}}{2n_e\hbar^3\pi^2}\frac{\sqrt{E}}{\exp(E/T_e-\eta)+1}, \tag{7}$$

where η is the degeneracy parameter, and $f_e(E)dE$ is the probability for finding electrons with energy between E and $E+dE$. Degeneracy parameter η can be obtained by equation normalization,

$$\int \frac{(2m_e)^{3/2}}{2n_e\hbar^3\pi^2}\frac{\sqrt{E}dE}{\exp(E/T_e-\eta)+1} = 1. \tag{8}$$

Here, Eq. (8) defines η as a function of n_e and T_e. The occupancy function is the measure of the proportion of states occupied at energy E, and is given by,

$$f_o(E) = f_e(E)/g_e = (E)\frac{1}{\exp(E/T_e-\eta)+1}, \tag{9}$$

where $g_e(E) = (2m_e)^{3/2}\sqrt{E}/2n_e\hbar^3\pi^2$ is the density of states between E and $E+dE$. From Eq. (8), $\eta=-\infty$ corresponds to the classical limit in which the distribution functions become Maxwell distributions. In the zero temperature limit, $\eta = E_F/T_e$ and $\eta=\infty$, with $E_F = (3\pi^2 n_e)^{2/3}\hbar^2/2m_e$ of the Fermi energy. Note, $\eta=\infty$ is the fully degenerate limit, in which all particles are at energies below or equal to the Fermi energy, and the occupancy function becomes a step function: $g(E)=1$ with $E\le E_F$; and $g(E)=0$ with $E>E_F$. For non-Maxwellian distributions, temperature and average energy no longer satisfy $T_e = (2/3)E_{\rm ave}$, where $E_{\rm ave}$ is the average kinetic energies. In the case of the Fermi-Dirac distribution, particles retain an energy even in the $T_e=0$ limit. This is because, lower energy states have limited capacity and become fully occupied, so that remaining particles occupy energy states higher than the ground state.

Particles with a defined distribution function can be initialised in the PIC code. Ions or atoms obeying Maxwellian distributions are initialised using the Box-Muller transform method [23], which is proven to be computationally efficient. For distributions which are everywhere integrable, the probability density function, i.e., the distribution function, can be integrated to the cumulative density function $\int_0^x f(x')dx' = F(x)$. The cumulative density function is normalised, with $F(0)=0$ and $\lim_{x\to\infty}F(x)=1$. Inversion of the cumulative density function with $F^{-1}(u)=x$; $u\in(0,1)$ represents a parametrisation of the real number line between 0 and 1 into the space of the variable. Randomly generated values of u, uniformly distributed and in the domain of $F^{-1}(u)$, generate values of x that occur with frequencies determined by the original probability density function.

As the Fermi-Dirac distribution is not integrable, this process cannot be done analytically, and numerical methods of calculating the inverse cumulative distribution function must be used. In the LAPINS code, we employ Hormann and Leydold's algorithm [24] to numerically compute the energy values in order to initialise degenerate particles. In this method, the domain of $F^{-1}(u)$ is split into equally spaced sub-intervals and a cubic Hermite polynomial $H_i(u)$ is used to interpolate values of E for given u, with $F(E)_i \leq u \leq F(E)_{i+1}$.

For given value of particle energy E, components of each particle's velocity are calculated as follows. For an isotropic distribution of velocities, each energy can be thought of as defining a radius of a sphere in velocity space. When scaling a value with $u_e = \sqrt{2E/m_e}$, the velocity components are given by: $u_x = u_e\sqrt{1-r^2}\cos(\phi)$, $u_y = u_e\sqrt{1-r^2}\sin(\phi)$, and $u_z = u_e r$, where $r \in (-1, 1)$ and $\phi \in (0, 2\pi)$.

Before computing the energy values in order to initialise degenerate particles, degeneracy parameter η in Eq. (7) need to be solved out in advance. Given initial temperature T_e and electron density n_e in Eq. (8), the calculation of η can be done only by using numerical method. Here in LAPINS code, a golden section search method [25] is used for the minimisation of the root sum square, and calculation of η.

When initialised, as shown in Fig. 2, we have plotted the energy distribution of free electrons for solid aluminium at $T_e = 1$ eV, $T_e = 5$ eV and $T_e = 10$ eV, respectively. Distributions produced by Fermi-Dirac statistics are displayed by triangles, and by Maxwell statistics are displayed by diamonds. For solid aluminium, the average ionization degree is $\bar{Z} = 3$ at room temperature, and the free electron density can be as high as 1.8×10^{23} cm^{-3}. Following Eq. (8), the Fermi energy is $E_F = 11.2$ eV. As shown in Fig. 2, when temperature is well below Fermi energy, Fermi-Dirac distributions significantly depart from Maxwell distributions, and states with energies lower than Fermi energy, are fully occupied. When temperature is well above Fermi energy, Fermi-Dirac distribution become close to the Maxwell distributions. Actually, at high temperatures with $T_e \gg E_F$, Fermi-Dirac statistics will become identical to Maxwell statistics, and the proportion of states occupied with any energy E is zero, $f_o(E) \to 0\ \forall E$.

However, particles in PIC simulations are treated as distinguishable classical macro-particles, and initialised Fermi-Dirac distributions would relax to Maxwell distributions due to particle-particle and particle-field interactions. To prevent this, one must take into account Pauli exclusion principle. Here, we assume all processes which lead to changes in energies of degenerate particles, such as particle-particle scatterings or acceleration/deceleration by electromagnetic fields, must be constrained by Pauli exclusion principle. This principle prevents degenerate particles being scattering into an energy state E if that state is already occupied. The occupancy function, Eq. (9), is the measure of the proportion of states occupied

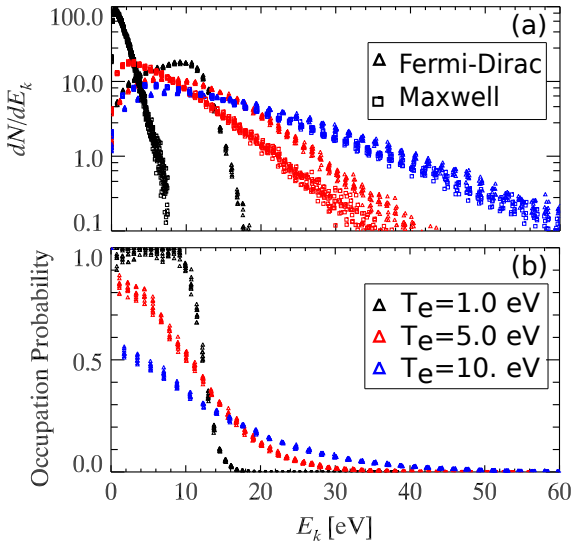

FIG. 2. (color online) The LAPINS PIC code producing a Fermi-Dirac distribution of free electrons for solid density aluminium at $T_e = 1$ eV, $T_e = 5$ eV and $T_e = 10$ eV, respectively. (a) It is shown against Maxwell and Fermi-Dirac distributions with the same parameters. (b) The occupation function sampled from the simulation distribution function.

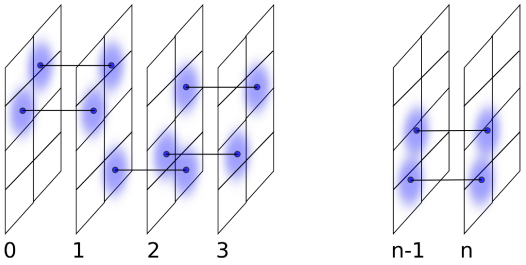

FIG. 3. (color online) Schematic presentation of the two-fold interpretation method. Here, n is the size of array containing distribution functions. See text for further explanations.

at energy E. As f_o takes values between 0 and 1, from the point of view of PIC/MC simulations, it indicates whether a particular energy changing process should be blocked or not. The probability of accepting a change to final energy should be $1 - f_o(E)$, therefore fully occupied states admit no more particles. The probability of accepting a new energy change depend on the degeneracy, therefore for the classical limit with $\eta \to \infty$, $f_o(E) \to 0$ is reproduced for any E.

As reflected in Eq. (9), f_o depends on the local distribution function. Within PIC/MC simulations, the local distribution function can be generated by collecting all particles within a computational cell. In order to generate a smooth f_o as a function of particle energy, the number of particles in each cell should be on order of magnitudes 10^3 or even larger. For a typical PIC simulation with computational grids at 10^3, it will quickly become computationally intractable. To avoid such an

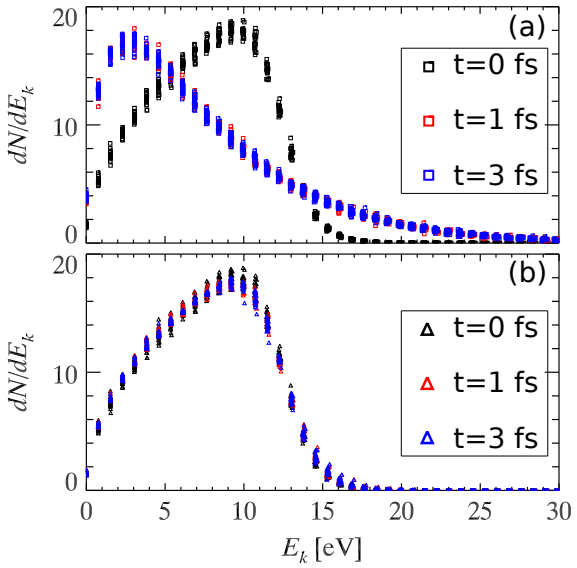

FIG. 4. (color online) (a) With initial Fermi-Dirac distribution, it has relaxed to Maxwell distributions after 1 fs. (b) Also with initial Fermi-Dirac distribution, when including Pauli exclusion principle, it sustains within the entire simulation duration. Simulation parameters are the same with as displayed in Fig. 2 with $T_e = 1$ eV.

incredible simulation burden and simultaneously generate a smooth distribution or occupation function, we here propose a two-fold interpretation method.

The schematic presentation of this two-fold interpretation method is displayed in Fig. 3. Attaching each computational cell, we define an array with size, for example, $n = 50$. This array is used to contain the local distribution function of degenerate particles. The cut-off energy here is defined as, for example, $E_c = 2E_F$, where $E_F = (3\pi^2 n_e)^{2/3}\hbar^2/2m_e$ is the Fermi energy. Note, this cut-off energy E_c is a global constant. Once initially defined, it is shared by each array during the entire simulation duration. The array index is therefore defined as $E_k = kd_E$, with $k \in [0, n]$, $d_E = E_c/n$, and $n = 50$. Within PIC simulations, for a degenerate particle with an arbitrary weight w, only if the particle's energy is located within $0 < E < E_c$, the particle is used to fill an array. Locate the nearest two elements, k and $k+1$, with $E_k < E < E_{k+1}$, and then fill them with $F_k = w(1-\delta)S(\mathbf{r}-\mathbf{R})$ and $F_{k+1} = w\delta S(\mathbf{r}-\mathbf{R})$. Here, $\delta = (E - kd_E)/d_E$ and $S(\mathbf{r}-\mathbf{R})$ is the particle shape function, with which $\sum_{i,j,k} S[\mathbf{r} - (i\mathbf{x} + j\mathbf{y} + k\mathbf{z})] = 1$ is satisfied. Note the particle shape function used here shares the same idea with the high order interpolation algorithms for current assignment and force interpolation widely used in PIC codes in order to suppress numerical noises. This two-fold interpretation method could significantly avoid incredible simulation burden by using less particles per cell and simultaneously generate a smooth distribution or occupation function.

In PIC simulations, in order to include the Pauli exclusion principle on changes in particle energy with the final energy E_f, a random number R is generated. With $R \in (0, 1)$ and E_f: block the change if $R < f_o(E_f)$; accept the change if $R > f_o(E_f)$. For two-body processes, such as fermion-fermion scatterings, there is a natural extension. With finial energies E_{f1} and E_{f2}: block the change, if $R < f_o(E_{f1}) + f_o(E_{f2}) - f_o(E_{f1}) \cdot f_o(E_{f2})$. Here, we always set $f_o(E_f) = 0$ for non-degenerate particles and degenerate particles with final energy larger than the cut-off energy E_c. For ideal plasmas, $f_o(E) = 0\ \forall E$, changes in particle energy is no longer blocked.

In order to benchmark the implemented Pauli block method, a simulation box is divided into $10 \times 10 \times 10$ computational cells bounded by periodic conditions, with each cell contains 100 macro-electrons. Here, energy distribution of free electrons for solid aluminium with $T_e = 1$ eV is displayed in Fig. 4. As shown in Fig. 4 (a), an initial Fermi-Dirac distribution relaxes to Maxwell distributions after only 1 femtosecond. However when taking into account Pauli exclusion principle, as shown in Fig. 4 (b), Fermi-Dirac distribution sustains within the entire simulation duration. Note, the simulation speed is only slightly affected by including Pauli exclusion principle. This is because, the same interpretation method is used throughout the code for both current assignment and force interpretations.

B. Collisions

In the LAPINS code, treatment of collisions is based on Monte Carlo binary collision approximation. This method was originally proposed by Takizuka and Abe [20], and then extended several times, for example, by Sentoku [19]. In this approach, particles are randomly paired with each other in close proximity and scattered with collisions, each one of which conserves energy and momentum. Apart from conservation, the greatest strength of this approach is the ability to work with any distribution function, especially those which depart appreciably from a Maxwell distribution.

In practical implementation, the Monte Carlo binary collision model requires knowledge of the momentum transfer cross sections. In the partial wave calculation [26], this momentum transfer cross section can be obtained by numerical solution of the Schroedinger equation for a well defined potential. In the original work of Lee and More [27], the Thomas-Fermi potential was taken as an approximate candidate. Recently, more rigorous approach has been proposed by Starrett [26] that includes correlations with electrons and ions surrounding the central scatterer through the quantum fluid equations. Comparing with these numerically calculated cross sections, here in the LAPINS code, screened Coulomb cross section with approximate cut-off parameters is used. This is because, our goal is to invent an simulation method for degenerate plasmas for practical applications, and we need a simple yet approximately ac-

curate method for calculating cross sections.

To calculate Coulomb cross section, one of the practical approaches, as used by Takizuka [20] and Sentoku [19], is to sum binary collisions over a distance of the order of the Debye length. Under the Coulomb potential of $1/r$, the differential cross-section reads,

$$\sigma(\theta) \sim 1/\sin^4(\theta/2), \tag{10}$$

and the Coulomb logarithm reads,

$$L \sim \int_0^\pi \sin\theta \sin^2(\theta/2)\sigma(\theta)d\theta \sim \ln[\sin(\theta/2)]|_0^\pi \tag{11}$$

This integration is not a convergent value, when $\theta \to 0$. While in plasmas, the potential of a charged particle should be screened. When b, i.e., the minimum impact parameter, is larger than λ_D, the potential is artificially set to be zero. Therefore, the lower limit θ_min of scattering angle is obtained when $b = \lambda_\mathrm{D}$, i.e., $\theta_\mathrm{min}/2 = b/\lambda_\mathrm{D}$. Thus we have $L \sim \ln(\lambda_D/b)$. In this model, for high energy density plasmas with b close to or even larger than λ_D, the Coulomb logarithm is artificially cut-off with a value equal to 2.0.

However instead of the above method, a rigorous way is to sum binary collisions with all surrounding particles using the screened potential $\exp(-r/\lambda_\mathrm{D})/r$. Acted by this screened potential, under Born approximation, the differential cross-section can be analytically obtained with

$$\sigma(\theta) \sim 1/[\sin^2(\theta/2) + \xi]^2, \tag{12}$$

where ξ is noting but the ratio of minimum impact parameter and the Debye length. $\xi = b_\mathrm{min}/\lambda_D$. The minimum impact parameter is set by the classical distance of closest approach. This gives

$$b_\mathrm{min} = Z_a Z_b e^2/m_{ab}u_{ab}^2, \tag{13}$$

Here, Z_a and Z_b are the charge number of particle a and particle b, m_{ab} and u_{ab} are their reduced mass and relative velocity. However, at high energy, b_min is set by the uncertainty principle. We have

$$b_\mathrm{min} = \lambda/2 = \hbar/m_{ab}u_{ab}, \tag{14}$$

here λ is the de-Broglie wavelength. The Coulomb logarithm $L \sim \int_0^\pi \sin\theta \sin^2(\theta/2)\sigma(\theta)d\theta$ by applying the new differential cross-section is integrable with

$$L \sim \ln[1 + 2\eta - \cos(\theta)]|_0^\pi \sim \ln[(1+\eta)/\eta]. \tag{15}$$

This expression of Coulomb logarithm will converge to $L = \ln(\lambda_\mathrm{D}/b)$ when $b \ll \lambda_\mathrm{D}$ for ideal plasmas. For high energy density plasmas, this expression of Coulomb logarithm reduces to zero.

In our model, the screen is only determined by the Debye length. This length, following Debye-Huckel theory, can be written as,

$$\frac{1}{\lambda_D^2} = \frac{4\pi n_e e^2}{kT_e} + \frac{4\pi n_i e^2 \bar{Z}^2}{kT_i}, \tag{16}$$

where T_e and T_i are the electron and ion temperature, n_e and n_i are the electron and ion density, and $\bar{Z}$ is the average ionization degree. Note, the ion contribution is dominant for plasmas containing heavy atoms. The degeneracy correction to the screening is to multiply the first term on the right hand of Eq. (16) by a factor $F'_{1/2}/F_{1/2}$, i.e., the logarithm of derivative of the Fermi integral,

$$F_j(x) = \int_0^\infty \frac{x^j dx}{1 + \exp(x - \eta)}, \tag{17}$$

where η is the degeneracy parameter defined by Eq. (8). The second term remains unchanged. According to the original work of Brysk, Campbell and Hammerling [28], such a degeneracy correction can be approximated to

$$\frac{1}{\lambda_D^2} = \frac{4\pi n_e e^2}{(T_e^2 + E_F^2)^{1/2}} + \frac{4\pi n_i e^2 \bar{Z}^2}{T_i}. \tag{18}$$

This approximation matches the numerical calculation of the factor $F'_{1/2}/F_{1/2}$ within 5%, giving negligible error in the logarithm.

For electrons of Fermi-Dirac distributions, diagnosing the electron temperature is non-trivial. Here, the average electro energy is

$$\bar{E} = \frac{3\sqrt{\pi}}{8}\frac{T_e}{n_e}\frac{(2m_e T_e)^{3/2}}{\hbar^3\pi^2}F_{3/2}(\eta). \tag{19}$$

For ideal plasmas, i.e., $\eta \to -\infty$, $\bar{E} = (3/2)T_e$, and for fully degenerate plasmas, i.e., $\eta \to \infty$, $\bar{E} = (3/5)E_F$. Within PIC simulations, Eq. (19) can be approximated by $\bar{E} \sim \bar{E}_\mathrm{PIC} = \sum_i w_i\epsilon_i/\sum_i w_i$, where ϵ_i is the energy for each single macro-particle and w_i is the corresponding weight. The first term on the right hand of Eq. (16) can therefore be directly approximated as $4\pi n_e e^2/\bar{E}_\mathrm{PIC}$, also giving negligible error in the logarithm.

For projectile moving in the plasmas, the static Debye length needs to be replaced by a corresponding dynamical value. According to Zwicknagel [29], this dynamical Debye length reads $\tilde{\lambda}_D = \lambda_D(1 + m_{ab}u_{ab}^2/T_e^2)$. In the LAPINS code, this dynamical correction is used as default, although we have about a factor 2 difference in the logarithmic scale. This is because, having one general formula for stopping and relaxation problems is useful for practical applications, such as the laser-solid interactions, which contains the fast particle stopping and thermalization simultaneously.

In the simulations, the frequency of scattering between particle a and particle b is

$$\nu_{ab} = \frac{2\pi e^2 Z_a Z_b n_\mathrm{min} L}{m_{ab}^2 u_{ab}^3}, \tag{20}$$

where L is the Coulomb logarithm, and n_min is the minimum density for particle species a and b. After calculating ν_{ab} for a given pair of particles, the velocity or energy change within a scattering is evaluated following

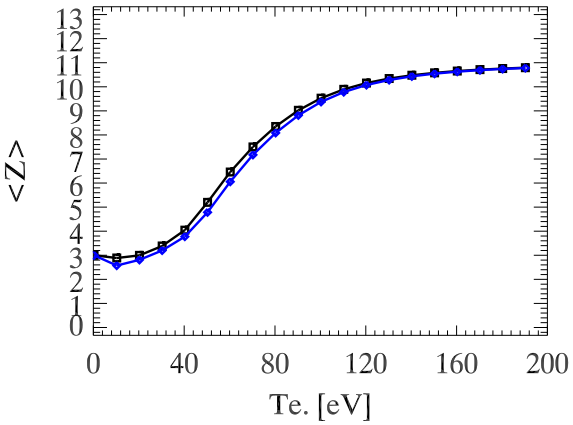

FIG. 5. (color online) The average ionization degree of solid aluminium as a function of temperature. Black square line is the one without degeneracy corrections, and blue diamond line is the one with degeneracy corrections.

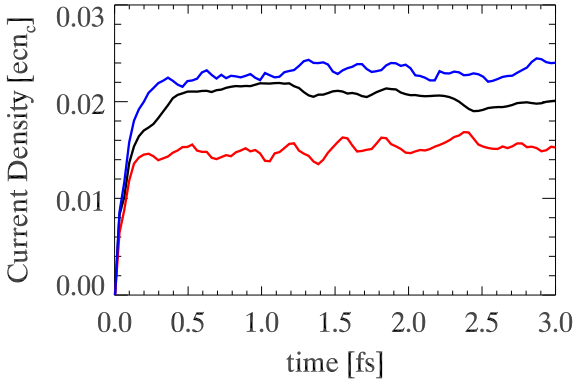

FIG. 6. (color online) The evolutions of electron current density of a solid aluminium sample as functions of time, when externally applying a small electric field. Here, black, red and blue curves are the ones with $T_e = 1$ eV, $T_e = 10$ eV and $T_e = 20$ eV, respectively.

the typical routine proposed by Takizuka and Abe [20]. However, in the LAPINS code, the change of velocity or energy needs to be constrained by the Pauli exclusion principle: block or accept depending on the local occupation function f_o.

C. Ionizations

In the LAPINS code, the treatment of ionization is divided into two parts: field ionization [30, 31] and impact ionization. As field ionization usually appears under low density plasmas, therefore, there is no need to take into account degeneracy corrections. For solid density plasmas, a dynamic ionization model was proposed by Wu [32], taking into account impact ionization, electron-ion recombination and ionization potential depression (IPD) by the shielding of surrounding plasmas. Here, we would suggest to include the degeneracy effect by correcting ionization potential with $P - \Delta P + E_F$, with P the isolated ionization potential [33], ΔP the IPD correction [34, 35], and E_F the Fermi Energy. As there is no space to contain the newly ionized electrons with energy lower than E_F, the minimum kinetic energy of a newly ionized electron must be higher than E_F. Numerical experiments, Fig. 5, have showed that such a degeneracy correction would slightly decrease the ionization cross section and therefore the average ionization degree with temperature comparable to and lower than E_F.

IV. BENCHMARKS

In this section, the code is applied to several benchmark simulations, including electronic conductivity for aluminium, equilibration of cold fuel shell and alpha particles in inertial confinement fusion, and rapid heating of solid aluminium by intense laser beams.

A. Electronic conductivity of aluminium

The calculation of electronic conductivity in high energy density plasmas is a challenging problem. One approach is to use DFT-MD coupled with Kubo-Greenwood formalism [8, 9]. This method is thought to be curate but is limited in the problems it can be applied to due the significant computational expense.

Another class of methods starts from the Boltzmann equation and introduces a relaxation-time approximation in which electrons are scattered from ions. The question then becomes calculating the electron-ion cross sections. To calculate the electron-ion cross section in high energy density plasmas, one needs to define an electron-ion scattering potential. How this definition is made strongly affects the resulting conductivities. Recently, a new quantum potential is defined by Starrett [26], who couple average atom models to the relaxation-time approximation. This potential includes correlations with electrons and ions surrounding the central scatterer through quantum Ornstein-Zernike equations [36]. Results indicates that this new potential leads to quite accurate conductivity predictions when to compared to DFT-MD simulations.

As the underling frame of the LAPINS code is Boltzmann equation coupled with Maxwell equations, therefore, for electronic conductivity calculation, the relaxation-time approximation algorithm is naturally recovered by applying a small external electric field on a plasma sample. Free electrons are accelerated by this small electric field, and simultaneously experience collisions with ions. When reaching steady state, the conductivity is evaluated as $\sigma = \mathbf{J}/\mathbf{E}$, with $\mathbf{J}$ and $\mathbf{E}$ of current density and electric field.

In Fig. 6, we have plotted the evolution of electron current density of a solid aluminium sample, when externally exposing in a small electric field. This current density increases at initial time due to the acceleration of electric field and then reaches saturation due to the anti-

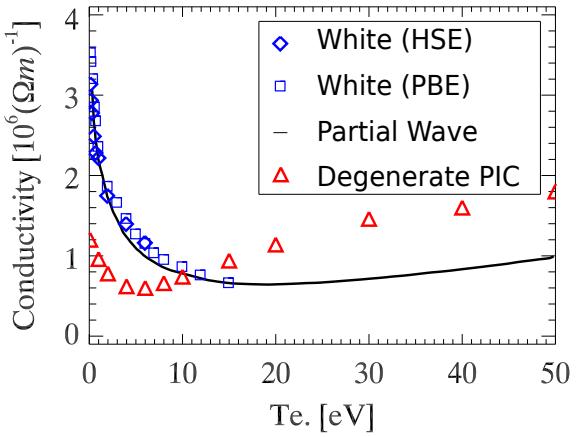

FIG. 7. (color online) Electrical conductivity of solid aluminium. Degenerate PIC simulation method are compared with full quantum mechanical calculations, including both partial wave method from Starrett [26] and Kubo-Greenwood DFT-MD method from Witte [37].

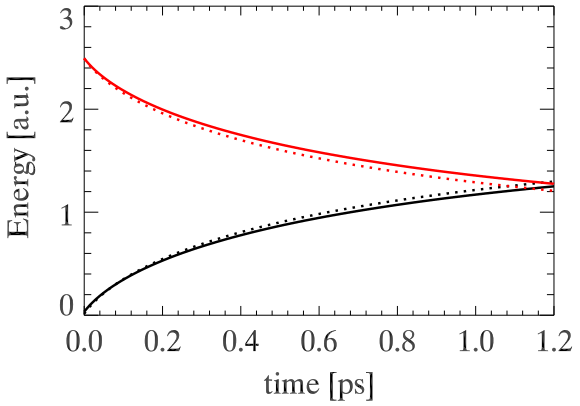

FIG. 8. (color online) An equilibration scenario with parameters approximately similar to inertial confinement fusion: starting temperatures of electrons, deuterium and tritium are 12.5 eV, the density is $n_{\rm D} = n_{\rm T} = 1.2 \times 10^{24}$ cm^{-3}; $n_\alpha = 0.01 n_{\rm D}$ and $n_e = 2.4 \times 10^{24}$ cm^{-3}, α particles have an initial energy of 3.54 MeV. Solid line is for degenerate simulation, and dashed line is for non-degenerate simulation.

balance forces from collisional scatterings. Here, black, red and blue curves represent evolutions at different temperatures, with $T_e = 1$ eV, $T_e = 10$ eV and $T_e = 20$ eV, respectively. In Fig. 7, electronic conductivity calculated by the LAPINS code are compared with full quantum mechanical calculations, including both partial wave method from Starrett [26] and Kubo-Greenwood DFT-MD method from Witte [37]. It is shown that the LAPINS code could generally produce accurate conductivity predictions when to compared to full quantum mechanical simulations. The departure is due to the simplified cross-section used in the PIC code.

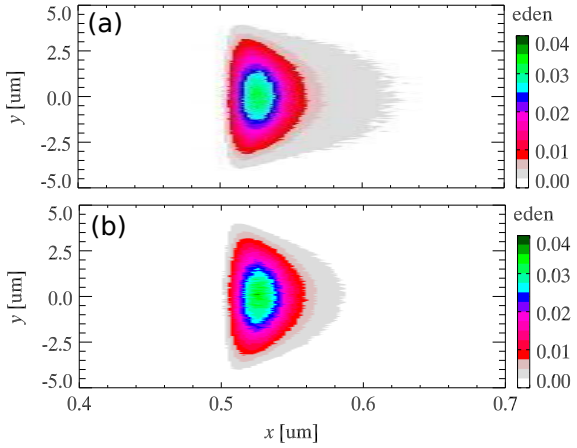

FIG. 9. (color online) Simulation of intense laser interaction with a solid aluminium sample, displaying the energy density distribution for free electrons. The laser intensity is of 10^{16} W/cm^2. (a) and (b) correspond to degenerate and non-degenerate simulations.

B. Equilibration of cold fuel shell and alpha particles

Here, we present an application of the LAPINS code to the interaction between fusion produced alpha particles and background high density deuterium-tritium plasmas. In ICF, the yield of neutrons is particularly sensitive to electron-ion equilibration. Simulations of direct-drive implosions have shown a 10% difference across several different models of temperature relaxation [38]. The distribution of fusion produced alpha particles is highly non-Maxwellian, however the LAPINS code with the implemented collision method is capable of modelling such an complex interaction. Fig. 8 shows a simulation with parameters approximately similar to ICF: an isotropic flux of mono-energetic fusion produced alpha particles interacting with a cold fuel shell of deuterium, tritium and electrons. For comparison, the numerical simulation is also shown against the non-degenerate equilibration case. The degenerate simulation predicts a significantly slow relaxation rate, due to the reduction of collisions by Pauli exclusion principle.

C. Rapid heating of solid aluminium

Here, we present an application of the LAPINS code to the interaction of intense laser beam with a solid aluminium. Fig. 9 shows a the energy density distribution for free electrons. For comparison, the numerical simulation is also shown against the non-degenerate equilibration case. The degenerate simulation predicts a significantly larger hot spot, due to enhanced range of thermal electrons influenced by Pauli exclusion principle.

V. DISCUSSIONS AND CONCLUSIONS

To summarize, in this paper, we have invented a self-consistent kinetic approach for simulation of plasmas with an arbitrary degeneracy level. With this approach, degenerate particles are initialized according to a Fermi-Dirac distribution function, and non-degenerate particles are initialized following typical Maxwell distribution function. The equation of motion of both degenerate and non-degenerate particles are governed by long range collective electromagnetic fields and close particle-particle scatterings with degeneracy corrections. Especially, evolutions of degenerate particles are also constrained by the Pauli exclusion principle. The new code might find great applications in ICF, astrophysical, and laboratory astrophysical studies. The method invented in this paper is applicable for plasmas with any degeneracy, however it needs to be carefully evaluated when applying to strong coupling plasmas.

ACKNOWLEDGMENTS

This work was supported by Science Challenge Project (No. TZ2016005), National Natural Science Foundation of China (No. 11605269) and National Basic Research Program of China (Grant No. 2013CBA01504).

[1] J. Lindl, Development of the indirect-drive approach to inertial confinement fusion and the target physics basis for ignition and gain, Physics of Plasmas 2, 3993 (1995).
[2] Y. Setsuhara, H. Azechi, N. Miyanaga, H. Furukawa, R. Ishizaki, K. Nishihara, M. Katayama, A. Nishiguchi, K. Mima, S. Nakai, Laser and Particle Beams 8, 609 (1990).
[3] J. P. Cox, R. T. Giuli, Principles of Stellar Structure Volume II: Applications to Stars, Gordon and Breach Science Publishers, 1968.
[4] F. N. Beg, A. R. Bell, A. E. Dangor, C. N. Danson, A. P. Fews, M. E. Glinsky, B. A. Hammel, P. Lee, P. A. Norreys. and M. Tatarakis, Phys. Plasmas 4, 447 (1997).
[5] P. K. Patel, A. J. Mackinnon, M. H. Key, T. E. Cowan, M. E. Foord, M. Allen, D. F. Price, H. Ruhl, P. T. Springer, and R. Stephens, Phys. Rev. Lett. 91, 125004 (2003).
[6] W. Bang, B. J. Albright, P. A. Bradley, E. L. Vold, J. C. Boettger, and J. C. Fernandez, Phys. Rev. E 92, 063101 (2015).
[7] G. M. Dyer, A. C. Bernstein, B. I. Cho, J. Osterholz, W. Grigsby, A. Dalton, R. Shepherd, Y. Ping, H. Chen, K. Widmann, and T. Ditmire, Phys. Rev. Lett. 101, 015002 (2008).
[8] M. P. Desjarlais, J. D. Kress, L. A. Collins, Phys. Rev. E 66 (2002) 025401.
[9] T. Sjostrom, J. Daligault, Phys. Rev. E 92 (2015) 063304.
[10] B. Holst, M. French, R. Redmer, Phys. Rev. B 83 (2011) 235120.
[11] M. French, T. R. Mattsson, Phys. Rev. B 90 (16) (2014) 165113.
[12] S. X. Hu, L. A. Collins, T. R. Boehly, J. D. Kress, V. N. Goncharov, S. Skupsky, Phys. Rev. E 89 (2014) 043105.
[13] M. P. Desjarlais, C. R. Scullard, L. X. Benedict, H. D. Whitley, R. Redmer, Phys. Rev. E 95 (2017) 033203
[14] Mark R. Krumholz, Richard I. Klein, and Christopher F. McKee, The Astrophysical Journal 754, 71 (2012).
[15] Nick Higginbottom, Christian Knigge, Knox S Long, James H Matthews, Stuart A Sim, Henrietta A Hewitt, Monthly Notices of the Royal Astronomical Society, 479, 3651 (2018).
[16] C. K. Birdsall, A. B. Langdon, Plasma Physics via Computer Simulation, Taylor and Francis, New York, 2005.
[17] D. Wu, W. Yu, S. Fritzsche, and X. T. He, Phys. Rev. E 100, 013207 (2019).
[18] D. Wu, W. Yu, Y. T. Zhao, D. H. H. Hoffmann, S. Fritzsche, and X. T. He, Phys. Rev. E 100, 013208 (2019).
[19] Y. Sentoku, A. J. Kemp, Journal of Computational Physics 227, 6846 (2008).
[20] T. Takizuka and H. Abe, J. Comput. Phys. 25, 205 (1977).
[21] D. Wu, X. T. He, W. Yu, and S. Fritzsche, Phys. Rev. E 95, 023207 (2017).
[22] A. E. Turrell, M. Sherlock, S. J. Rose, Journal of Computational Physics 249, 13 (2013).
[23] G. E. P. Box, M. E. Muller, A note on the generation of random normal deviates, The Annals of Mathematical Statistics 29, 610 (1958).
[24] W. Hoermann, J. Leydold, Continuous random variate generation by fast numerical inversion, ACM Transactions on Modelling and Computer Simulation 13, 347 (2003).
[25] W. H. Press, S. A. Teukolsky, W. T. Vetterling, B. P. Flannery, Numerical Recipes in C++, Cambridge University Press, 2007.
[26] C. E. Starrett, Potential of mean force for electrical conductivity of dense plasmas, High Energy Density Physics 25, 8 (2017).
[27] Y. T. Lee and R. M. More, Phys. Fluids 27, 1273 (1984).
[28] H. Hrysk, P. M. Campbell, and P. Hammerling, Plasma Physics 17, 473 (1975).
[29] G. Zwicknagel, C. Toepffer. and P. G. Reinhard, Phys. Rep. 309 117 (1999).
[30] M. V. Ammosov, N. B. Delone, and V. P. Krainov, Sov. Phys. JETP 64, 1191 (1986).
[31] D. Wu, B. Qiao, X. T. He, C. McGuffey and F. N. Beg, Phys. Plasmas 21, 123118 (2014).
[32] D. Wu, X. T. He, W. Yu, and S. Fritzsche, Phys. Rev. E 95, 023208 (2017).
[33] Refer to http://physics.nist.gov/PhysRefData/ASD/ for ionization energy data.
[34] G. Ecker and W. Kroll, The Phys. Fluids 6, 62 (1963).
[35] John C. Stewart and Kedar D. Pyatt, Astr. Phys. J. 144, 1203 (1966).
[36] J. Chihara, J. Phys. 3, 8715 (1991).
[37] B. B. L. Witte, P. Sperling, M. French, V. Recoules, S. H. Glenzer, and R. Redmer, Physics of Plasmas, 25, 056901, (2018).
[38] B. Xu, S. X. Hu,, Physical Review E 84, 016408 (2011).